Hierarchical-structure-dependent high ductility of electrospun polyoxymethylene nanofibers

Article *in* Journal of Applied Polymer Science · September 2018

DOI: 10.1002/app.47086

7 authors, including:

Ruirui Hu
Tsinghua University
12 PUBLICATIONS **67** CITATIONS
SEE PROFILE

Enlai Gao
Wuhan University
39 PUBLICATIONS **269** CITATIONS
SEE PROFILE

Zhiping Xu
Tsinghua University
192 PUBLICATIONS **5,059** CITATIONS
SEE PROFILE

Luqi Liu
National Center for Nanoscience and Technology
76 PUBLICATIONS **3,279** CITATIONS
SEE PROFILE

ATLAS
MATERIAL TESTING SOLUTIONS

1915
Solar
Determinator®

1927
Original
Weather-Ometer®

1954
Xenotest® 150

1977
Ci65 Weather-Ometer®

1995
Ci4000
Weather-Ometer®

TODAY
The Ci4400
Weather-Ometer®

Our Latest Milestone. The Atlas Ci4400.

For over 100 years, we've revolutionized the science of weather durability testing. The new Atlas Ci4400 Weather-Ometer® is our most advanced instrument yet, delivering unparalleled performance and value. With its simplified operation, unmatched uniformity, increased capacity and sleek design, the best-in-class just got even better. Learn more at **atlas-mts.com**.

AMETEK®
MEASUREMENT, COMMUNICATIONS
& TESTING

JOURNAL OF Applied Polymer SCIENCE

Hierarchical-structure-dependent high ductility of electrospun polyoxymethylene nanofibers

Ruirui Hu,[1,2] Enlai Gao,[3] Zhiping Xu,[3] Luqi Liu,[2] Guorui Wang,[2] Hongwei Zhu,[1] Zhong Zhang[2]

[1]State Key Laboratory of New Ceramics and Fine Processing, School of Materials Science and Engineering, Tsinghua University, Beijing 100084, China

[2]Chinese Academy of Science Key Laboratory of Nanosystem and Hierarchical Fabrication, National Center for Nanoscience and Technology, Beijing 100190, China

[3]Applied Mechanics Laboratory, Department of Engineering Mechanics, Tsinghua University, Beijing 100084, China

Correspondence to: L. Liu (E-mail: liulq@nanoctr.cn); Z. Zhang (E-mail: zhong.zhang@nanoctr.cn)

ABSTRACT: Two types of electrospun polyoxymethylene nanofibers with rough and smooth surface morphologies [rough fibers (RFs) and smooth fibers (SFs), respectively] were successfully prepared via the control of the electrospinning voltages. Mechanical tensile tests showed that the RF nonwoven mats exhibited a much higher elongation (440%) than the SFs (180%) without sacrifices in the stiffness and strength. Scanning electron microscopy characterization revealed that the large ductility of a single RF resulted from its unique multiple-necking mode, which was induced by its rippled structural features. In the meantime, the large ductility led to a high molecular orientation under tension and further improved the strength and toughness of the RF nonwoven mats. In comparison, the SF behaved in a single-necking deformation mode, and this led to a rapid rupture behavior. This surface-morphology-dependent mechanical behavior helped us to deeply understand the relationship between the structure and properties and should guide the development of high-performance materials for load-bearing applications. © 2018 Wiley Periodicals, Inc. J. Appl. Polym. Sci. **2018**, *135*, 47086.

KEYWORDS: electrospinning; fibers; mechanical properties; morphology

Received 3 May 2018; accepted 10 August 2018
DOI: 10.1002/app.47086

INTRODUCTION

Electrospinning has been recognized as a versatile processing technique that allows the production of ultrathin polymeric fibers with diameters down to the tens of nanometers.[1,2] In a typical electrospinning process, a high voltage is applied to eject a polymer jet to form a nanofiber mat as the solvent evaporates. Through the precise control of the various electrospinning parameters, electrospun fibers with hierarchical structures can be achieved.[3] For example, grounded collectors with different configurations facilitate the assembly of various nanofiber structures in terms of aligned fiber mats,[4,5] patterned mats,[6] and nanowebs.[7] Within these assembled structures, the individual electrospun fibers have displayed diverse structures, including flat-ribbon,[8] helical,[9] hollow,[10] pearl-necklace,[11] and core–shell[12] fibers, as determined by the humidity, viscosity, voltage, and so on. Further detailed characterizations have revealed the presence of nanopores[13] and nanoprotrusions[14] on individual fiber surfaces. Such hierarchical structural characteristics of electrospun fiber mats not only provide great flexibility in the modification of the properties of electrospun nanofibers but also enable a broad scope of applications in the fields of biomedicine,[15] filtration,[16] sensors,[17] catalysis,[18] and composites.[19]

Given the fact that both the functionality and durability of electrospun mats are ensured by their long-term mechanical stability, it is fundamentally important to investigate the overall mechanical properties of electrospun fibers. However, to date, investigations have mainly focused on the strength and modulus of the fibers, and the ductility has been taken into account less.[20–25] For instance, several methods, including mat twisting,[26] net crosslinking,[23] nanofiber alignment,[24] and single-walled carbon nanotube reinforcement,[25] have been proposed to prepare high-strength and high-stiffness electrospun nonwoven mats. As a matter of fact, a high strength and stiffness are always accompanied by defect-induced brittleness, and thus, it remains a great challenge to enhance the ductility of electrospun fibers without a loss in strength and stiffness.

In earlier studies, researchers have observed novel necking modes in terms of nanonecking and multiple necking in porous poly(methyl methacrylate)–montmorillonite electrospinning

Additional Supporting Information may be found in the online version of this article.

fibers[27] and poly(ethylene oxide) nanofibers.[28] Specifically, the nanopores on the fiber surface acted as stress concentrators to trigger the initiation of necking and finally led to large failure strain. Such unusual deformation behaviors provide valuable clues for overcoming the intrinsic brittleness and simultaneously endowing materials with a high strength and toughness.

In this study, we used polyoxymethylene (POM) as a reference because of its poor ductility. Through the adjustment of the electrospinning voltages, electrospun POM fibers with two different surface morphologies were prepared, namely, rough fibers (RFs) and smooth fibers (SFs). Tensile tests revealed that compared with the SF nonwoven mats with about 180% failure strain, the RF nonwoven mats showed a pronouncedly higher elongation up to 440% without sacrifices in the modulus and failure strength. Such unusual behaviors were further revealed by single-nanofiber mechanical tests. Our results imply that electrospun fibers with a rough surface morphology readily trigger multiple necking and lead to extremely high ductilities.

EXPERIMENTAL

Materials

POM with 10 wt % oxyethylene units was provided by Yunnan Yuntianhua Co., Ltd. (China). 1,1,1,3,3,3-Hexafluoro-2-propanol (HFIP) was purchased from Shanghai Aladdin Co., Ltd.

Preparation of the Electrospun POM Nanofiber Nonwoven Mats

A 5 wt % POM solution was prepared through the dissolution of POM granules in HFIP solvent at 40 °C with stirring for 2 h. The solution was immediately transferred to a 10 mL syringe to prevent the evaporation of HFIP. In the electrospinning process, the syringe was placed vertically so that the solution was fed by gravity. The distance from the needle tip to the grounded collector was fixed at 10 cm. The applied voltage was kept at 6 kV for the RFs and 15 kV for the SFs. The ambient temperature and relative humidity were maintain in ranges of 20–25 °C and 60–65%, respectively. The electrospun POM fibers were deposited onto a sheet of aluminum foil, and each mat was dried in a desiccator before use.

Preparation of Single Electrospun POM Nanofiber Samples

As illustrated in Scheme 1, first, an aluminum frame was used to collect aligned single nanofibers. Second, a piece of cardboard with a central circle window with a diameter of 11 mm was placed under the aluminum frame and moved upward to attach electrospun fibers, and then, single fibers were transferred onto the cardboard. Meanwhile, the partially aligned fibers in the cardboard were removed by tweezers. Finally, AB glue (modified acrylate resins, "A" component was mixed with "B" at a ratio of 1:1) was used to fix both ends of the fiber onto the cardboard.

Characterization of the Morphology and Deformation Process of the Electrospun POM Nanofibers

The morphology of the electrospun POM nanofibers was characterized by scanning electron microscopy (SEM; JSM-7500F) and transmission electron microscopy (TEM; Tecnai G2 20 S-TWIN). The deformation modes of the POM nonwoven mats were investigated by SEM at different strain levels.

Tensile Tests of the Electrospun POM Mats and Single Fibers

The tensile tests of the electrospun POM nonwoven mats and single fibers were performed with an Agilent T150 universal testing system at fixed strain rates of 2×10^{-3} and 1×10^{-3} s^{-1}, respectively. The nanofiber mats were cut into a rectangular shape (11×2 mm^2) and then adhered to a cardboard frame. The thickness of the fiber mat was measured by a micrometer.

Polarized Fourier Transform Infrared (FTIR) Spectroscopy

The molecular orientation was measured with a polarized FTIR spectrometer with a resolution of 2 cm^{-1}. Nonwoven POMs (RF and SF) at different strain levels were investigated.

Differential Scanning Calorimetry (DSC)

DSC measurements of the POM nonwoven mats were operated under the flow of N_2 gas at a heating rate of 10 °C/min from 25 to 220 °C, and the degree of crystallinity was estimated as the ratio of the melting heat of the mats to that of an assumed 100% crystalline POM sample.

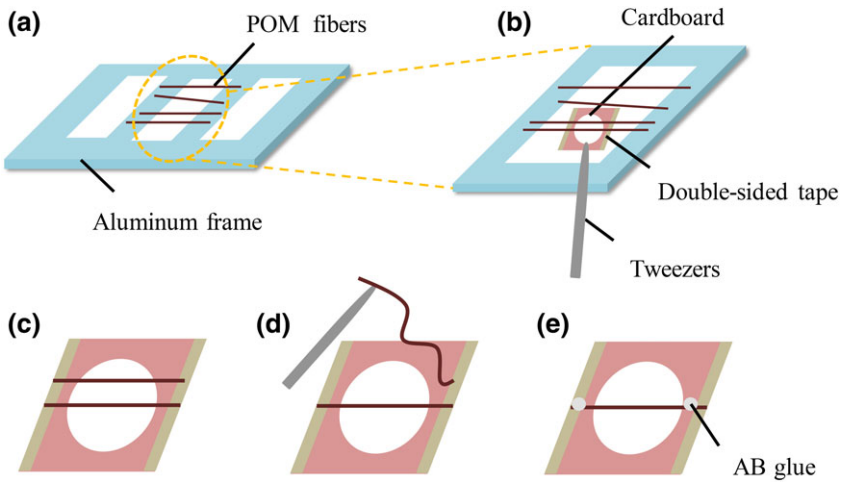

Scheme 1. Schematic of the preparation of single POM nanofiber samples for tensile testing. [Color figure can be viewed at wileyonlinelibrary.com]

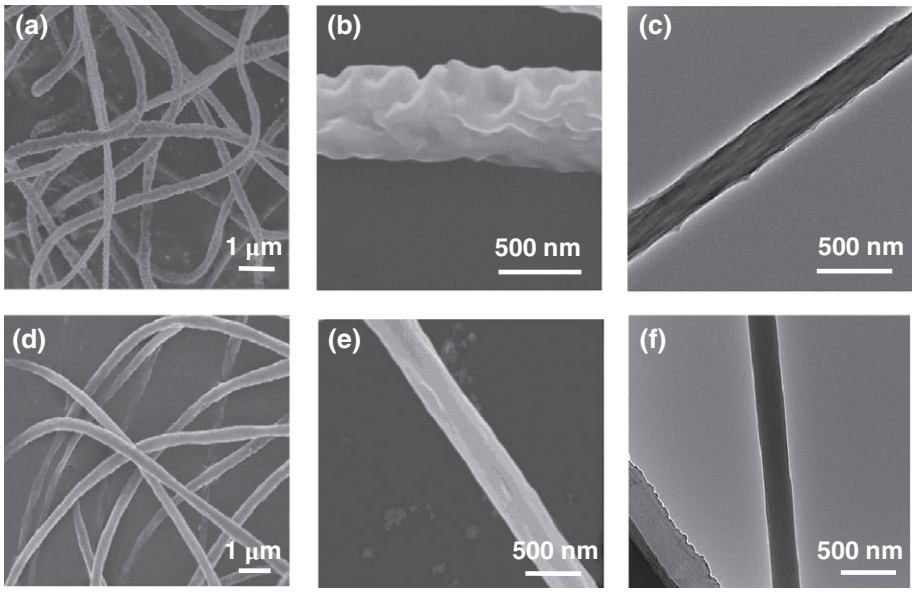

Figure 1. (a,b,d,e) SEM micrographs and (c,f) TEM micrographs of the electrospun POM nanofibers prepared at different electrospinning voltages: (a–c) 6 and (d–f) 15 kV.

RESULTS AND DISCUSSION

Characterization of the Electrospun POM Fibers

Electrospun nanofibers usually possess a smooth surface with a circular cross section. Depending on the electrospinning parameters, such as the concentration, temperature, humidity, and applied voltages, electrospun fibers with different surface morphologies can be produced.[29] Herein, POM fibers were prepared with a POM copolymer–HFIP solution as a feeding source, and the electrospinning conditions were changed to adjust the fiber morphology. Figure 1 shows the typical morphologies of electrospun POM fibers fabricated at different electrospinning voltages. RFs with highly dense pits or ripples over the surface were achieved at an electrospinning voltage of 6 kV [Figure 1(a–c)]. When the electrospinning voltage was increased up to 15 kV, the fiber surface became smooth, as shown in Figure 1(d–f). Statistical analysis based on more than 100 fibers of each sample indicated that the fiber diameters were predominately in the ranges of 500–600 nm for RFs and 400–500 nm for SFs. Because of the high vapor pressure of the HFIP solvent, the RF electrospun fibers with ripple features were attributed to the phase separation during the solvent-evaporation process.[29] The lower electrospinning voltage delayed polymer ejection and thus facilitated more evaporation of HFIP during the jet flight. As a result, enormous pits formed on the fiber surface. In contrast, a higher applied voltage led to a faster rate of polymer ejection, and hence, a shorter evaporation time resulted in an SF surface. Even though earlier studies have revealed the influence of the relative humidity of the atmosphere on the fiber morphology,[1,29] herein, we mainly focused on the applied voltage and its influence on the fiber morphology at a certain humidity.

It is well known that the mechanical performances of electrospun nanofibers are greatly affected by their crystal structure and crystallinity.[30] Previous work has confirmed that there are usually two types of crystalline phases in POM, including extended-chain crystals and folded-chain crystals.[31] Figure 2 shows the characteristic peaks at 897, 935, 1092, and 1235 cm^{-1}; these confirmed the presence of extended-chain crystals initiated by stretching during the electrospinning process. A small shoulder at 995 cm^{-1} was ascribed to the amorphous phase in the system. Furthermore, the crystalline contents of the nonwoven mats measured by DSC showed values of 41.4 and 42.0%, respectively, for RF and SF mats with the assumption that the melting heat of a 100% crystalline POM sample was 317.9 J/g.[32]

Mechanical Properties of the Electrospun POM Fibers

The tensile mechanical properties of the electrospun POM mats were determined by a uniaxial tensile tester. Figure 3a–c show the typical stress–strain curves of the electrospun POM nonwoven mats based on five samples. Both the RF and SF mats exhibited elastic behaviors at lower strain levels; this was followed by plastic deformation at higher strains. Figure 3(d) summarizes the overall tensile mechanical properties of the nonwoven mats, in which the tensile modulus and failure strength of the RF mats (29.0 ± 6.1 and 3.7 ± 0.3 MPa, respectively) were apparently higher than that of the SF mats (14.8 ± 1.6 and 2.8 ± 0.2 MPa, respectively). We attributed the relatively higher tensile modulus of the RF mats to the increased frictional force between neighboring individual electrospun fibers due to the rough surface morphology. Surprisingly, more than one time, the RF fiber mats exhibited a failure strain (440 ± 40%) that was higher than that of the SF mats (180 ± 30%). To the best of our knowledge, such an exceedingly high breaking strain of electrospun mats has only been reported in the polyurethane elastomer system (330%), whereas the maximum failure strain for brittle polymer nonwovens is usually less than 200%. For example, the elongations at break for poly(ethylene terephthalate) and poly(methyl methacrylate) were only 23 and 40% (as shown in Figure S1 and Table S1, Supporting Information). Furthermore, the RF mats also exhibited a relatively high toughness (12.6 ± 1.6 MJ/m^3; this was about a three-fold enhancement compared with that of the SF mats (4.1 ± 0.9 MJ/m^3. It should be emphasized that even the electrospun POM nonwoven mats exhibited a higher ductility than its

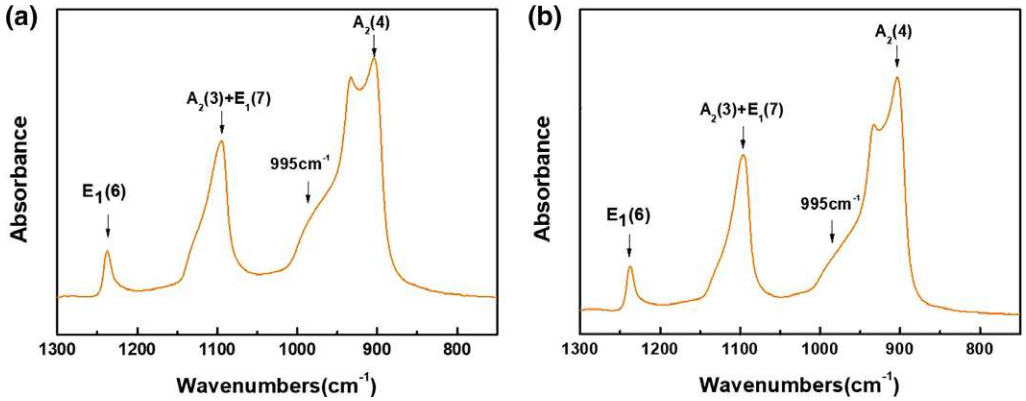

Figure 2. FTIR spectra of the electrospun POM nonwoven mats for the (a) RFs and (b) SFs. The bands due to the A_2 symmetry species have the transition dipole along the chain axis, and the infrared- and Raman-active E_1 bands have the transition dipole perpendicular to the chain axis. [Color figure can be viewed at wileyonlinelibrary.com]

counterparts (hot-pressed POM film, failure strain < 20%), and its tensile strength was at least one order of magnitude lower than that of the hot-pressed POM film because of the microporous characteristics of the nonwoven mats.

Because both the crystallization degree of the polymer and the electrospun fiber orientation in the RF and SF nonwoven mats were similar to each other, the observed distinct difference in ductility might have been related to the various surface

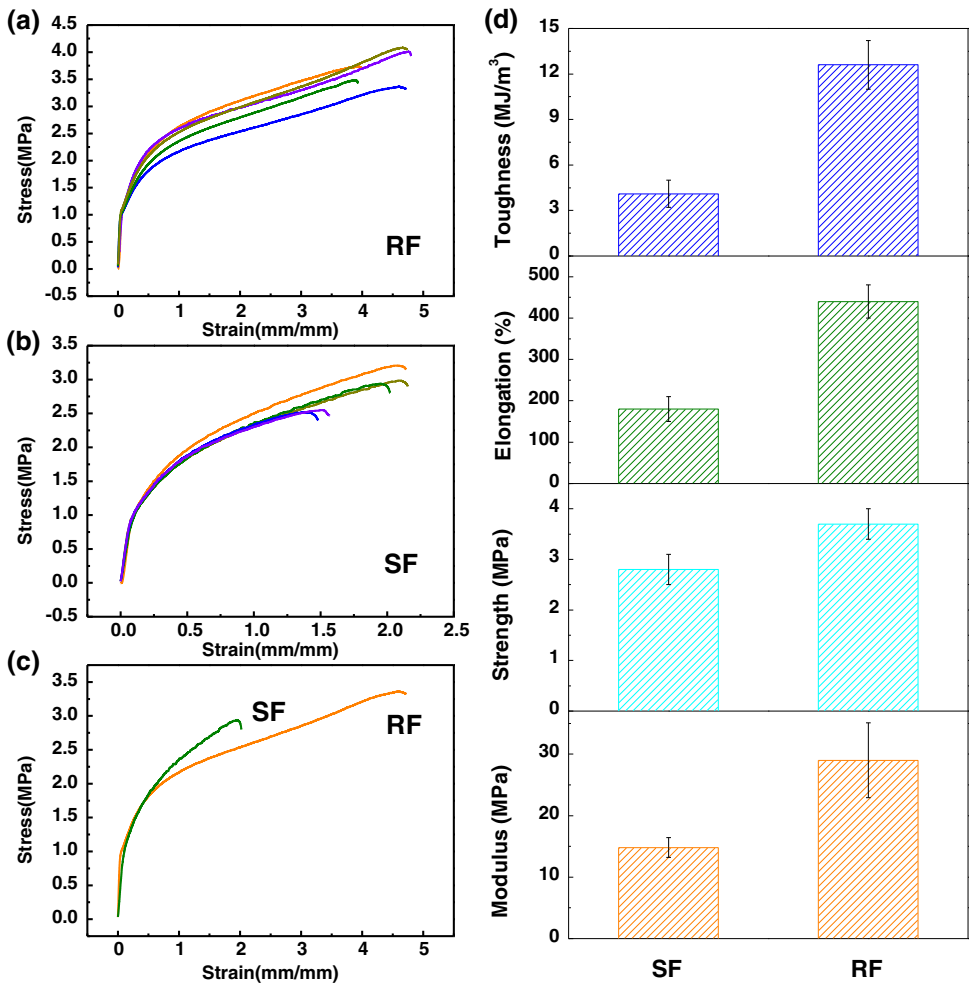

Figure 3. Tensile stress–strain results for the electrospun POM RF and SF mats: (a) RF and (b) SF. (c) Comparison of typical stress–strain curves for RF and SF. (d) Comparison of the mechanical properties of the RF and SF mats, including the modulus, strength, elongation, and toughness, as obtained from the stress–strain curves. [Color figure can be viewed at wileyonlinelibrary.com]

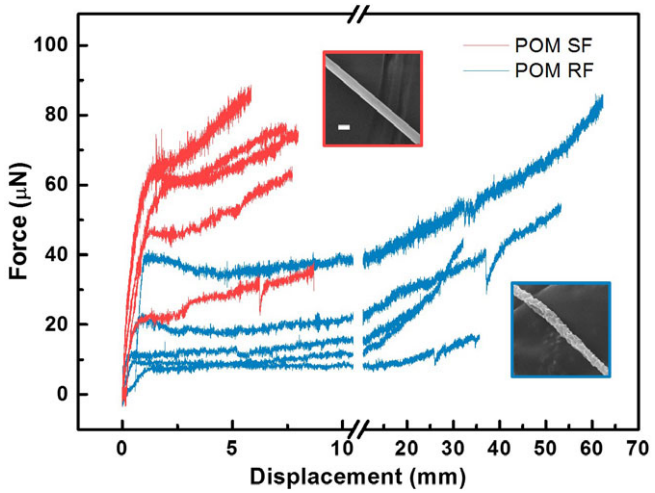

Figure 4. Force–displacement curves of single POM RFs and SFs (scale bar in the inset = 500 nm). [Color figure can be viewed at wileyonlinelibrary.com]

morphologies of the POM nanofibers. To deeply understand such structure-dependent mechanical behaviors, we studied the tensile properties of single POM fibers further. Figure 4 shows the force–displacements curves of single RF and SF nanofibers. Both curves exhibited a similar trend, with a linear region followed by a strain-hardening region. The average failure strain of the RF fibers reached 412 ± 144% on the basis of the measurement of five samples. Instead, the failure strain of the SF fibers was in the range 75 ± 10%. Even though the individual RF showed notable deviations in the failure stain, it was noteworthy that the RF possessed a much higher failure strain than the SF. Also, the trend of failure strain of single POM fibers was well consistent with that of nonwoven mats.

Deformation Mechanisms of the Electrospun POM Nanofibers

To explore the underlying deformation mechanism of the fibers and clarify its impact on the tensile properties of the nonwoven mats, POM nanofibers stretched at different strain levels were examined by SEM (Figure 5) and FTIR spectroscopy (Figure 6). As shown in Figure 5(a), in the initial state, the ripples were homogeneously distributed along the RF fiber surface. After 50% tensile stretching, nanoporous structures were formed because of the ripple-induced stress concentration [Figure 5(b)]. Interestingly, the rippled structures on the RF surface easily induced multiple stress concentrations along the fiber axis, and these uniformly spread along the whole fiber axis. When the stretch ratio was further increased to 100–200%, the nanopores tended to elongate along the axial direction [Figure 5(c)]. Eventually, the ligaments within the pores were highly stretched, and an extrusion of a 45 °cone was formed at the fractured end of fibers [-Figure 5(d,e)]. In contrast, the SF showed a single necking mode under tensile deformation [Figure 5(f)], which was followed by an even fracture surface [Figure 5(g)]. Such a deformation mode is a common phenomenon in thermoplastic polymers, where the weak point readily triggers stress concentration under tension and eventually leads to a rupture in the necking region.[33]

In addition to monitoring the evolution of the surface morphology on the basis of SEM, we also used polarized FTIR spectroscopy to reveal changes in the molecular orientations under tension. The dashed line in Figure 6 represents the parallel components of the IR beam, and the solid line corresponds to the perpendicular components. The molecular chains oriented along the stretching direction exhibited peaks at 1097 cm^{-1} [ν_a(COC) and δ(OCO)] and 897 cm^{-1} [ν_a(COC)] with a stronger parallel portion.[29] In our case, the RF nonwoven mats were stretched at elongations of 0, 200, and 350%, and the SF mats were stretched at 0, 100, and 200%, respectively. It was clear that the peak parallel intensities at 1097 and 897 cm^{-1} were significantly higher than those of the perpendicular components for both the RF and SF mats at a given applied strain level; this implied a pronounced molecular orientation of the fibers. To quantify such variations in the molecular orientation, we proposed a dichroic ratio (R), in

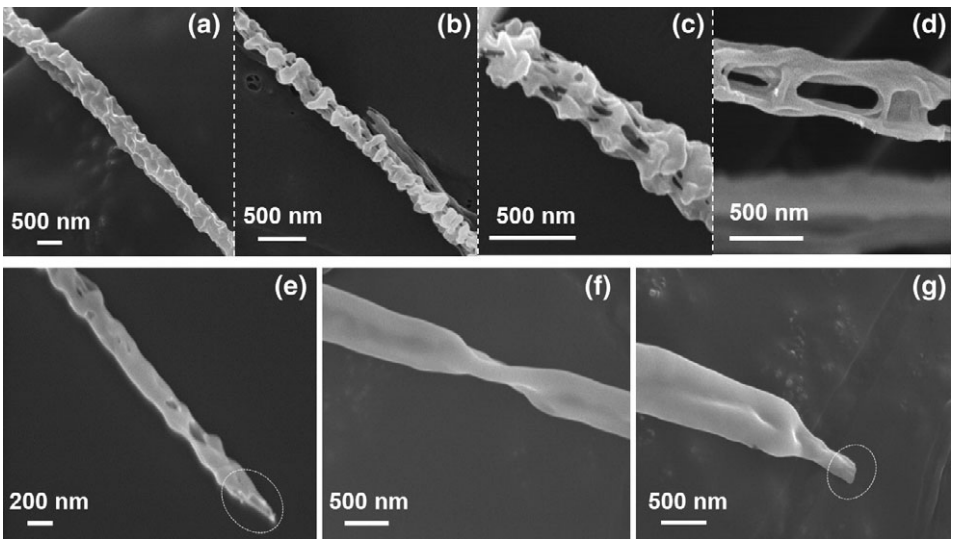

Figure 5. SEM micrographs of the deformation process and the failure modes for the POM RFs and SFs under uniaxial tension: (a–d) morphology evolution during the deformation process for the RFs at elongations of 0, 50, 200, and 400%, respectively; (e) an extrusion of a 45° cone for an RF; (f) necking for an SF; and (g) an even fracture for an SF.

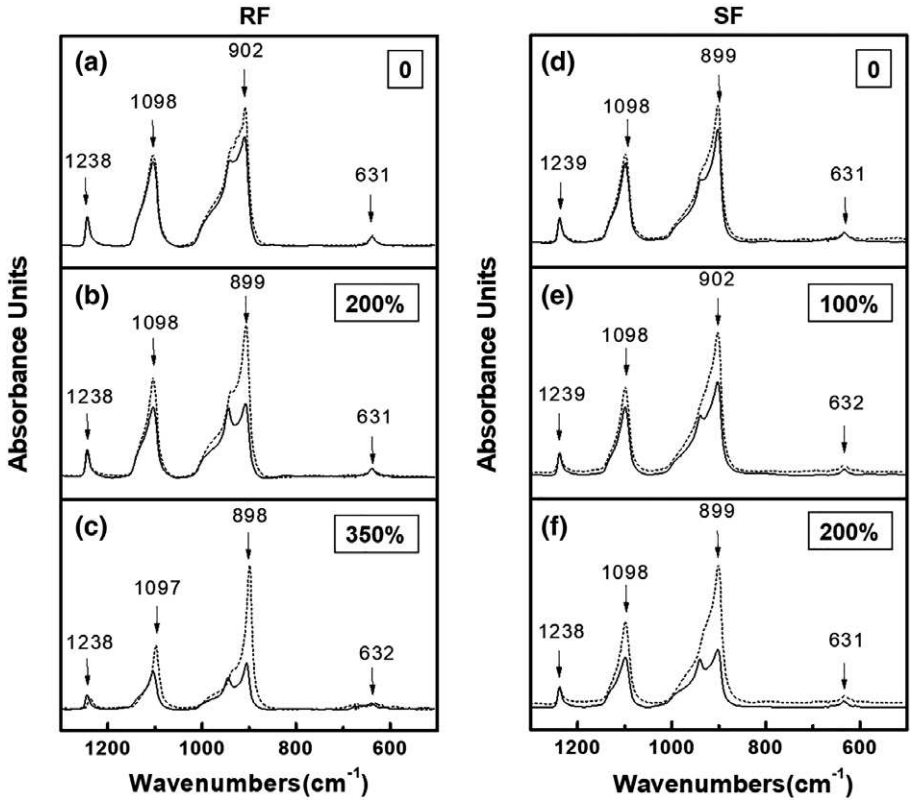

Figure 6. Polarized FTIR spectra of the electrospun POM nanofiber mats at different elongations: (a–c) RFs at 0, 200, and 350% and (d–f) SFs at 0, 100, and 200%. The dashed and solid lines represent the electric vectors of an IR beam parallel and perpendicular to the loading direction, respectively.

which *R* was defined as the ratio of IR absorbance of the parallel components to that of the perpendicular portion. A higher *R* indicates a better orientation of polymer chains. The calculated *R* values at 897 cm^{-1} increased to 3.1 and 2.4 at the break points for the RFs and SFs, respectively; this indicated the improved orientation degree of the molecules.

CONCLUSIONS

In conclusion, electrospun POM nanofibers with two different fiber morphologies were successfully prepared via the adjustment of the electrospinning voltages. Compared with SFs, having a smooth surface morphology, RFs, with a rough morphology, exhibited an extremely higher ductility under tension. This unique multiple-necking failure mode of the RFs provided an in-depth understanding of the relationship between the structure and mechanical properties and should guide the development of high-performance materials for load-bearing applications.

ACKNOWLEDGMENTS

This project was supported by the National Natural Science Foundation of China (contract grant number 21474023).

REFERENCES

1. Greiner, A.; Wendorff, J. H. *Angew. Chem. Int. Ed. Engl.* **2007**, *46*, 5670.
2. Dzenis, Y. *Science* **2004**, *304*, 1917.
3. Zander, N. *Polymers* **2013**, *5*, 19.
4. Li, D.; Wang, Y. L.; Xia, Y. N. *Nano Lett.* **2003**, *3*, 1167.
5. Theron, A.; Zussman, E.; Yarin, A. L. *Nanotechnology* **2001**, *12*, 384.
6. Li, D.; Ouyang, G.; McCann, J. T.; Xia, Y. N. *Nano Lett.* **2005**, *5*, 913.
7. Yang, S.; Wang, X.; Ding, B.; Yu, J.; Qian, J.; Sun, G. *Nanoscale* **2011**, *3*, 564.
8. Koombhongse, S.; Liu, W. X.; Reneker, D. H. *J. Polym. Sci. Part B: Polym. Phys.* **2001**, *39*, 2598.
9. Kessick, R.; Tepper, G. *Appl. Phys. Lett.* **2004**, *8*, 4807.
10. Li, D.; Xia, Y. N. *Nano Lett.* **2004**, *4*, 933.
11. Lim, J. M.; Moon, J. H.; Yi, G. R.; Heo, C. J.; Yang, S. M. *Langmuir* **2006**, *22*, 3445.
12. Wang, N.; Di, J. C.; Zhao, Y.; Song, Y. L.; Jiang, L. *Langmuir* **2010**, *26*, 11291.
13. Megelski, S.; Stephens, J. S.; Chase, D. B.; Rabolt, J. F. *Macromolecules* **2002**, *35*, 8456.
14. Lai, C.; Guo, Q.; Wu, X. F.; Reneker, D. H.; Hou, H. *Nanotechnology* **2008**, *19*, 195303.
15. Sahoo, S.; Toh, S. L.; Goh, *J. C. H. Biomaterials* **2010**, *31*, 2990.
16. Lim, H. S.; Baek, J. H.; Park, K.; Shin, H. S.; Kim, J.; Cho, J. H. *Adv. Mater.* **2010**, *22*, 2138.
17. Khalil, A.; Kim, J. J.; Tuller, H. L.; Rutledge, G. C.; Hashaikeh, R. *Sens. Actuators B* **2016**, *227*, 54.

18. Liu, Q.; Wang, Y.; Dai, L.; Yao, J. *Adv. Mater.* **2016**, *28*, 3000.
19. McCullen, S. D.; Stevens, D. R.; Roberts, W. A.; Ojha, S. S.; Clarke, L. I.; Gorga, R. E. *Macromolecules* **2007**, *40*, 997.
20. Lu, J. W.; Zhang, Z. P.; Ren, X. Z.; Chen, Y. Z.; Yu, J.; Guo, Z. X. *Macromolecules* **2008**, *41*, 3762.
21. Papkov, D.; Zou, Y.; Andalib, M. N.; Goponenko, A.; Cheng, S. Z. D.; Dzenis, Y. A. *ACS Nano* **2013**, *7*, 3324.
22. Wang, X.; Si, Y.; Wang, X.; Yang, J.; Ding, B.; Chen, L.; Hu, Z.; Yu, J. *Nanoscale* **2013**, *5*, 886.
23. Zhang, K.; Qian, Y.; Wang, H.; Fan, L.; Huang, C.; Yin, A.; Mo, X. *J. Biomed. Mater. Res. A* **2010**, *95*, 870.
24. Huang, C.; Chen, S.; Reneker, D. H.; Lai, C.; Hou, H. *Adv. Mater.* **2006**, *18*, 668.
25. Sen, R.; Zhao, B.; Perea, D.; Itkis, M. E.; Hu, H.; Love, J.; Bekyarova, E.; Haddon, R. C. *Nano Lett.* **2004**, *4*, 459.
26. Rein, D. M.; Shavit-Hadar, L.; Khalfin, R. L.; Cohen, Y.; Shuster, K.; Zussman, E. *J. Polym. Sci. Part B: Polym. Phys.* **2007**, *45*, 766.
27. Kim, G.-M.; Lach, R.; Michler, G. H.; Chang, Y.-W. *Macromol. Rapid Commun.* **2005**, *26*, 728.
28. Zussman, E.; Rittel, D.; Yarin, A. L. *Appl. Phys. Lett.* **2003**, *82*, 3958.
29. Kongkhlang, T.; Kotaki, M.; Kousaka, Y.; Umemura, T.; Nakaya, D.; Chirachanchai, S. *Macromolecules* **2008**, *41*, 4746.
30. Kongkhlang, T.; Tashiro, K.; Kotaki, M.; Chirachanchai, S. *J. Am. Chem. Soc.* **2008**, *130*, 15460.
31. Kobayashi, M.; Sakashita, M. *J. Chem. Phys.* **1992**, *96*, 748.
32. Iguchi, M. *Makromol. Chem.* **1976**, *177*, 549.
33. Kolluru, P. V.; Chasiotis, I. *Polymer* **2015**, *56*, 507.